Spin wave wavevector up-conversion in Y-shaped Permalloy structures

H.J. Jason Liu,[1, a)] Aron Guerrero,[1] Katherine E. Nygren,[2] Mitchell Swyt,[2] and Kristen S. Buchanan[2]

[1]*Department of Physics and Astronomy, Georgia Southern University, Statesboro, GA 30460*

[2]*Department of Physics, Colorado State University, Fort Collins, CO 80523*

[a)]*Author to whom correspondence should be addressed: hliu@georgiasouthern.edu*

Spin waves in micrometer-sized, patterned Y-shaped Permalloy structures were studied using micro-focus Brillouin light scattering (BLS) with a magnetic field applied in-plane. For in-plane magnetized thin films and microstrips, the dispersion relations depend on the angle of the magnetization with respect to the microstrip axis. BLS measurements show that spin waves generated in the two arms that form the top of the Y structure can be channeled into a longer magnetic microstrip that forms the base when the applied field is oriented perpendicular to the long axis of the base. In this configuration, the base supports surface spin waves. A comparison of the BLS data with micromagnetic simulations reveals that low-k spin waves generated by a microstrip antenna in the arms are converted to higher-k spin waves in the base, which may be useful for nanomagnonic applications.

Spin waves, also known as magnons, are propagating magnetic excitations that can be used to transmit information and carry out logic operations.[1,2] The past decade has seen an increase in research on magnonic devices.[3,4] These devices are ideal for microwave circuits and device miniaturization because spin waves span the gigahertz regime with wavelengths on the order of micrometers. A variety of devices have been proposed including spin wave-based logic devices that leverage interference effects.[5-13] For any such devices, understanding how spin waves come together at a junction is important, and new strategies for efficiently generating spin waves, especially short-wavelength/high-wavevector k spin waves, are needed to move devices into the nanoscale regime.

Oersted fields from microstrip antennas are commonly used to create spin waves. Antennas do not, however, scale favorably. The largest k that can be practically generated by an antenna is $k_{max} \sim \pi / w_{an}$ where w_{an} is the antenna width, and since the antenna resistance is also proportional to $1/w_{an}$, heating becomes a significant issue for nanoscale antennas.[14] Magnetic gratings[15] and parametric pumping[16] have been employed to obtain large-k spin waves; however, the former method relies on the use of a second material that must be carefully chosen to obtain a grating resonance frequency that matches the frequency of the desired k in the device, and the latter requires high microwave powers. Another approach to obtain high-k spin waves that avoids these complications is to exploit the characteristics of the dispersion relations for magnetic microstrips. For example, the dispersion relations of a magnetic microstrip are sensitive to geometric confinement,[17] and studies done on tapered waveguides show that the k of a traveling spin wave will increase as the waveguide width is reduced.[18] The dispersion relations for in-plane magnetized thin films and microstrips also differ depending on the angle between the static magnetization $\vec{M}_o$

and $\vec{k}$ due to the internal demagnetization fields[19], and, as will be shown, this provides new opportunities to manipulate k.

In this work, Brillouin light scattering (BLS) measurements done on Y-shaped magnetic structures show that channeling spin waves through a transition in the spin wave dispersion environment provides a new strategy to obtain higher-k spin waves. Spin wave propagation studies are often done in the magnetostatic surface wave or Damon Eshbach (DE) configuration with $\vec{M}_o \perp \vec{k}$. In fact, a method to maintain this configuration through curved waveguides to allow surface spin waves to travel around bends has been demonstrated,[20,21] and the changing dispersion environment can be used to selectively permit or block the passage of spin waves through branches of a Y-shaped structure.[21] Here, measurements and simulations are conducted that demonstrate that Y structures also offer new opportunities to increase k, since low-k spin waves generated in the arms of the Y will convert to higher-k surface spin waves in the DE-magnetized base.

Spin wave propagation was studied in a 40-nm thick $Ni_{80}Fe_{20}$ (Permalloy) Y-shaped structure made up of microstrips with widths of w = 2.7 μm, illustrated in Fig. 1(a). Throughout the work presented here, the Y structure is rotated by 90° counterclockwise, and the two arms that form the top of the letter "Y" are referred to as the top and bottom arms based on their locations after rotation. The top and bottom arms are at angles of $-45°$ and $+45°$ with respect to the x-direction, respectively, and the arms merge into the base of the Y that extends along the x-direction at a distance of x_0 = 1.75 μm. All distances x are measured from the edge of the antenna. A 300-nm thick, 10-μm wide gold microstrip antenna, separated from the Permalloy structure by a 100-nm thick SiO_2 insulating layer, was used to excite spin waves. An external magnetic field of $\mu_0 H$ = 60 mT was applied in the $+y$-direction and spin waves were detected with micro-focus BLS.[22-24] An objective (magnification 100x, numerical aperture = 0.75) is used to focus a laser

(wavelength of 532 nm) on the structure with a spatial resolution of approximately 300 nm, and the BLS signal is obtained by analyzing the backscattered light using a 6-pass tandem Fabry-Perot interferometer. The BLS signal was monitored as a function of the microwave frequency f supplied to the antenna to excite spin waves in the top and bottom arms, and the sample position was scanned with respect to the BLS probe laser to obtain two-dimensional spatial maps of the spin wave intensities.

Micromagnetic simulations were conducted using MuMax3[25] and compared to the experimental results. Simulations were done with a static magnetic field of $\mu_0 H$ = 60 mT for three cases: a long, straight 40-nm thick and 2.7-μm wide Permalloy microstrip with H applied in-plane and at 90° and 45° to the the long axis of the microstrip, and a Y-shaped structure with the same dimensions as the sample. These geometries will be referred to as the 90°, 45°, and Y cases, respectively. Material parameters appropriate for Permalloy were used: saturation magnetization M_s = 8 × 10^5 A/m, exchange A_{ex} = 1.3 × 10^{-11} J/m, a damping parameter of α = 0.01, and anisotropy was neglected. Dynamic magnetic fields were applied in-plane and perpendicular to the antenna axis within a 2-μm wide region; the antenna width was reduced to 100 nm to obtain spin wave dispersion relations. For the straight microstrip (90° and 45° cases), the antenna axis is set parallel to H, while for the Y-structure the antenna is oriented as shown in Fig. 1(a) and simulations were performed with H along y and misaligned by an angle of $-3°$ (i.e., $H_x = -H\sin(3°)$). Cells of 21 × 21 × 40 nm^3 were used. This is small compared to the wavelengths of interest and selected simulations repeated with half-sized cells yield the same results. A broadband sinc pulse was used to obtain the amplitude response as a function of frequency and spin wave dispersion relations. To understand the spin wave excitation patterns, simulations using a sinusoidal excitation field at the frequency of the peak response amplitude were also done and spin wave mode maps were obtained

by analyzing the magnetization over one period after a steady state response was reached (after 50 periods).

Figure 1(b) shows BLS measurements as a function of f obtained at x = 1 μm on each arm of the Y structure, and Fig. 1(c) shows the corresponding dataset obtained in the base of the Y at x = 5 μm at the midpoint of the microstrip (y = 0). The BLS counts in Figs. 1(b) and (c) are integrated counts over frequencies near f minus the corresponding integrated background counts obtained with the driving frequency turned off, also normalized by a reference signal. A single peak is observed for each of the top and bottom arms (Fig. 1(b)) at 7.47 $\pm$ 0.05 GHz and 7.34 $\pm$ 0.05 GHz, respectively. The signal in the base of the Y, in contrast, shows two broad peaks: a lower frequency peak that is centered at 6.37 $\pm$ 0.05 GHz and a higher frequency peak that extends from 7.3 to 7.8 GHz and overlaps with the signals observed in the arms.

Figure 1(d) shows micromagnetic simulations for the considered cases (90°, 45°, and Y) where the amplitudes of the Fourier transform of the z-component of the magnetic responses are shown as a function of f. Single peaks are observed for each case. The peaks for the 45° and Y cases are both at f = 7.25 GHz, which is close to the peaks observed in the arms (Fig. 1(b)) and the higher frequency peak observed in the base (Fig. 1(c)). The peak for the 90° case is at 6.35 GHz, which overlaps with the lower frequency peak observed in Fig. 1(c). This suggests that the lower frequency peak in Fig. 1(c) is due to spin waves that are excited in the base of the Y by the long-range Oersted fields of the antenna. Notably the higher frequency peak in Fig. 1(c) (7.3 to 7.8 GHz) is absent for the 90° case but present for the Y case, hence the high frequency peak in Fig. 1(c) is due to spin waves that have traveled into the base from the arms.

The peak frequencies observed for the top and bottom arms (Fig. 1(b)) are slightly different. Additional simulations show that a 200 nm variation in w, the experimental uncertainty

in w, leads to a 0.03 GHz frequency difference, while a misalignment of H by $\pm 3°$, the experimental uncertainty, leads to a shift of 0.09 GHz as well as a change in the amplitude that is comparable to what is observed experimentally. Therefore a misalignment of H by $\sim 3°$ is likely the cause of the differences in the signals between the two arms.

Figure 2(a) shows a two-dimensional spatial BLS scan of the Y-structure taken at f = 7.40 GHz, a frequency between the peaks of the two arms (Fig. 1(b)). Strong spin wave signals are observed in the arms that proceed past the junction, confirming that the signals generated in the arms propagate into the base. Although the spin wave intensities decrease with increasing x (Fig. 2(b)), the signal is above background out to the farthest measured distance (x = 7 μm). Simulations of the spin wave amplitudes (Fig. 2(c)) show that the spin waves propagate considerably farther to the right, the direction that includes the junction and base (positive x), as compared to the left, where the microstrips continue at 45° with respect to H (negative x). The signal vs. +x shows periodic decreases in intensity in the base at intervals of approximately 6 μm due to interference of width-quantized spin wave modes,[26] and a dip in the experimental signal is observed at a similar distance as compared to the first dip in the simulations (x = 5 μm).

Spin wave dispersion relations were calculated using micromagnetic simulations for the 90° and 45° cases (Figs. 3(a) and (b), respectively). The width of the antenna region was reduced to 100 nm to obtain a broader range of excited k_L, where k_L is the wavevector parallel to the microstrip axis, and dispersion relations were obtained by taking two-dimensional Fourier transforms of the out-of-plane component of the magnetization m_z vs. x and time. The spin wave dispersion relations in Fig. 3 show the available states at a given frequency as well as the relative excitation amplitudes of the allowed modes. The strongest responses in Fig. 3(a) and (b) are the lowest-order, width-quantized modes, and the weaker responses are higher-order, (odd only)

width-quantized modes. For the 90° case (Fig. 3(a), the DE geometry), continuous dispersion relations are obtained that agree with analytical calculations that assume quantization of the wavevectors along w.[19,26] The analytical theories that have been developed for microstrips are for high symmetry field directions so Fig. 3(b) only includes micromagnetic simulations.

Unlike the 90° case, the dispersion relations for the 45° case (Fig. 3(b)) are made up of sets of disconnected sections, which suggests that there are additional quantization effects. As shown in animations included as Supplemental Materials, the spin wave modes have backward volume characteristics, which is consistent with the slopes (negative for $k_L > 0$ and positive for $k_L < 0$) of the bright sections that make up the lowest-order dispersion relation. The frequency of the strongest peaks in Fig. 1(d) (f = 7.25 GHz, white dashed lines in Figs. 3(a) and (b)) corresponds to $k_L \sim 0$ for the 45° case and k_L = 1.1 rad/μm for the 90° case, hence spin waves excited at the peak frequency of the 45°-oriented arms must shift to higher k_L in order to propagate past the junction of the Y. The dispersion curves in Fig. 3 suggest that increasing f will lead to similar up-conversion in k_L and consequently a larger k_L in the base. Analytical calculations presented in the Supplemental Materials show that up-conversion magnitudes of >70 rad/μm are expected for smaller w.

Simulations of the spin wave modes at f = 7.25 GHz were done to further understand the mode conversion process in the Y structures. Figures 3(c) and (d) show amplitude maps of the modes and corresponding snapshots of m_z at a fixed time for H along the antenna and misaligned by $-3°$, respectively. The dark/bright/dark contrast across the microstrip width in the inset of Fig. 3(c), e.g., at x = 5 μm, and the bumps observed in Fig. 2(c) are due to interference of two odd width-quantized modes (n = 1 and 3) beyond the junction. The central bright area has a larger magnitude than the dark areas at $x = 5$ μm due to constructive interference in the center of the

microstrip (also seen in animations, Supplemental Materials). The approximate k_L obtained from analysis of the inset to Fig. 3(c) is 2.1 rad/μm, which matches the k_L for the n = 3 mode in the dispersion relation (Fig. 3(a)).

The amplitude vs. frequency response suggests that experimentally H is slightly misaligned by $-3°$, and Figure 3(d) shows that the misalignment of H leads to a slight difference in excitation amplitudes in the two arms, which is consistent with experimental results (Fig. 2a). The experimental data in Fig. 2(a) demonstrate that the generated spin waves continue into the base, which is consistent with the simulations, however, it is difficult to compare the excitation patterns directly in this region due to the limited scan range in the experiment. Interestingly, Fig. 3(d) (and the corresponding animation in the Supplemental Materials) shows an even n = 2 width-quantized excitation, a mode that is not directly excited by an antenna, which suggests that the field angle can provide a means to control the dominant mode.

The Y structures may offer excitation efficiency advantages over direct excitation by an antenna. In Fig. 1(d), the peak amplitudes for the 45° case is more than a factor of two higher as compared to the 90° case. These simulations have the same excitation field and microstrip length and this amplitude difference reflects a difference in the excitation efficiencies. (The Y structure simulations cover a larger area so the amplitude cannot be directly compared to the other cases). The excitation efficiency for spin waves is lower in the magnetostatic backward volume wave configuration (H at 0°) as compared to the DE configuration (H at 90°)[27,28] in the absence of a change in the antenna orientation. Here the torque is larger for the 45° case because the antenna is tilted, but the excitation area is increased by less than a factor of two over the 90° case, hence additional quantization effects may also contribute to the increased amplitude for the 45° case, as suggested by the dispersion relation (Fig. 3(b)).

In summary, micro-focus BLS measurements and micromagnetic simulations show that spin waves excited in the arms of a Y-shaped Permalloy structure will converge and continue past the junction, where measurable signals were detected out to $x = 7$ μm. The spin waves are able to propagate past the junction because states are available at the excitation frequency in both the arms and the base of the Y, and furthermore, since the states in the base have a larger k as compared to the antenna-excited spin waves in the arms, the spin waves undergo up-conversion of k. The results further suggest that the antenna-based excitation efficiency for spin waves in the arms of the Y structure is larger than for the DE geometry, likely due to confinement effects, and mode selection is also possible through small changes to the angle of H. Spin wave dispersion calculations suggest that it should be possible to reach wavevectors of greater than 70 rad/μm, hence these results have important implications for the development of nanomagnonic devices.

Supplementary Materials

See supplementary materials for animations of the spin wave amplitudes and analytical calculations of the up-conversion potential.

Acknowledgments

We thank Justin Dickovick for help with fabricating sample holders. We acknowledge the use of photolithography facilities supported by the National Science Foundation under Grant #NSF-DMR 1727044. Work at Colorado State University was supported by the W. M. Keck Foundation (simulations, measurements) and the National Science Foundation DMR Grant No. 1709525 (fabrication). We also acknowledge support for A. G. provided by the McNair Scholars Program at Georgia Southern University.

Data Availability

The data that support the findings of this study are available from the corresponding author upon reasonable request.

References

[1] A. Khitun and K. L. Wang, Superlattices Microstruct. **38**, 184 (2005).

[2] M. P. Kostylev, A. A. Serga, T. Schneider, B. Leven, and B. Hillebrands, Appl. Phys. Lett. **87**, 153501 (2005).

[3] A. Barman, G. Gubbiotti, S. Ladak *et al.*, J. Phys. Condens. Matter Phys. (2021).

[4] A. Mahmoud, F. Ciubotaru, F. Vanderveken, A. V. Chumak, S. Hamdioui, C. Adelmann, and S. Cotofana, J. Appl. Phys. **128**, 161101 (2020).

[5] N. Sato, K. Sekiguchi, and Y. Nozaki, Appl. Phys. Express **6**, 063001 (2013).

[6] K. Nanayakkara, A. Anferov, A. P. Jacob, S. J. Allen, and A. Kozhanov, IEEE Trans. Magn. **50**, 11 (2014).

[7] S. Klingler, P. Pirro, T. Brächer, B. Leven, B. Hillebrands, and A. V. Chumak, Appl. Phys. Lett. **106**, 212406 (2015).

[8] K. Nanayakkara, A. P. Jacob, and A. Kozhanov, J. Appl. Phys. **118**, 163904 (2015).

[9] M. Balinskiy, D. Gutierrez, H. Chiang, Y. Filimonov, A. Kozhevnikov, and A. Khitun, AIP Adv. **7**, 056633 (2017).

[10] G. Csaba, Á. Papp, and W. Porod, Phys. Lett. A **381**, 1471 (2017).

[11] T. Fischer, M. Kewenig, D. A. Bozhko, A. A. Serga, I. I. Syvorotka, F. Ciubotaru, C. Adelmann, B. Hillebrands, and A. V. Chumak, Appl. Phys. Lett. **110**, 152401 (2017).

[12] A. Papp, W. Porod, A. I. Csurgay, and G. Csaba, Sci. Rep. **7**, 9245 (2017).

[13] M. Balynskiy, H. Chiang, D. Gutierrez, A. Kozhevnikov, Y. Filimonov, and A. Khitun, J. Appl. Phys. **123**, 144501 (2018).

[14] A. Papp, G. Csaba, H. Dey, M. Madami, W. Porod, and G. Carlotti, Eur. Phys. J. B **91**, 107 (2018).

[15] H. Yu, O. d' Allivy Kelly, V. Cros, R. Bernard, P. Bortolotti, A. Anane, F. Brandl, F. Heimbach, and D. Grundler, Nat. Commun. **7**, 11255 (2016).

[16] H. Kurebayashi, O. Dzyapko, V. E. Demidov, D. Fang, A. J. Ferguson, and S. O. Demokritov, Appl. Phys. Lett. **99**, 162502 (2011).

[17] S. O. Demokritov, *Spin wave confinement*. (Pan Stanford Publishing, 2009).

[18] V. E. Demidov, M. P. Kostylev, K. Rott, J. Münchenberger, G. Reiss, and S. O. Demokritov, Appl. Phys. Lett. **99**, 082507 (2011).

[19] B. A. Kalinikos and A. N. Slavin, J. Phys. C Solid State Phys. **19**, 7013 (1986).

[20] K. Vogt, H. Schultheiss, S. Jain, J. E. Pearson, A. Hoffmann, S. D. Bader, and B. Hillebrands, Appl. Phys. Lett. **101**, 042410 (2012).

[21] K. Vogt, F. Y. Fradin, J. E. Pearson, T. Sebastian, S. D. Bader, B. Hillebrands, A. Hoffmann, and H. Schultheiss, Nat. Commun. **5**, 3727 (2014).

[22] T. Sebastian, K. Schultheiss, B. Obry, B. Hillebrands, and H. Schultheiss, Front. Phys. **3**, 35 (2015).

[23] S. O. Demokritov and V. E. Demidov, IEEE Trans. Magn. **44**, 6 (2008).

[24] F. Kargar and A. A. Balandin, Nat. Photonics (2021).

[25] A. Vansteenkiste, J. Leliaert, M. Dvornik, M. Helsen, F. Garcia-Sanchez, and B. V. Waeyenberge, AIP Adv. **4**, 107133 (2014).

[26] V. E. Demidov, S. O. Demokritov, K. Rott, P. Krzysteczko, and G. Reiss, Phys. Rev. B **77** (2008).

[27] U. K. Bhaskar, G. Talmelli, F. Ciubotaru, C. Adelmann, and T. Devolder, J. Appl. Phys. **127**, 033902 (2020).

[28] H. J. J. Liu, G. A. Riley, and K. S. Buchanan, IEEE Magn. Lett. **6**, 4000304 (2015).

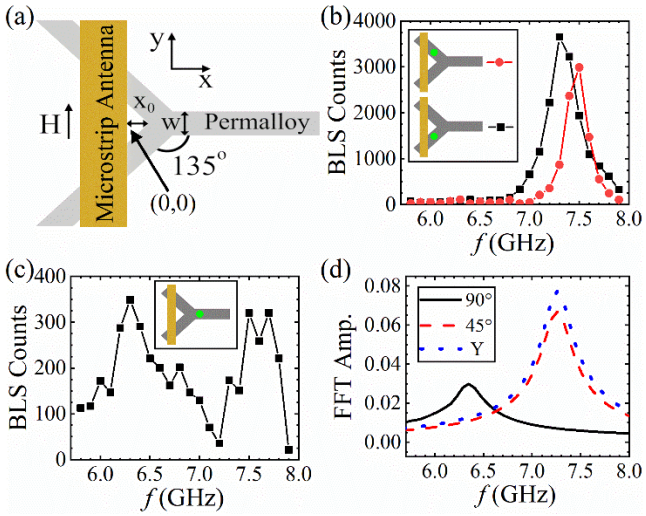

Figure 1: (a) Illustration of the sample and measurement setup. The Oersted field generated by the gold microstrip antenna was used to excite spin waves in the Permalloy Y-shaped structure and the dynamic response of the structure was probed by BLS using a focused laser spot. (b) Normalized BLS counts as a function of f measured at a distance of x = 1 μm from the edge of the antenna in the top and bottom arms of the Y structure, and (c) at the vertical center of the base of the Y at x = 5 μm, just to the right of where the base begins. The lines connecting the data points are provided to guide the eye. (d) Simulations of the amplitude vs. frequency response for a straight microstrip with H at 90° and 45° (90° and 45° cases), and for the Y structure (Y case).

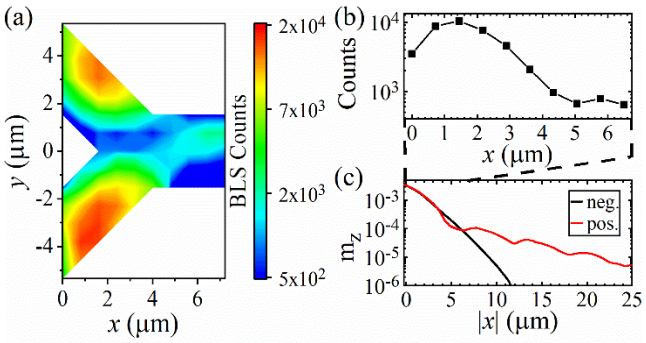

Figure 2: (a) Two-dimensional spatial BLS scan showing spin wave propagation in the Y structure for f = 7.40 GHz. (b) BLS counts from (a) integrated over y and shown as a function of x. The lines connecting the data points are provided to guide the eye. (c) The amplitude response integrated over y for simulations of the mode at f = 7.25 GHz, the peak frequency in Fig. 1(d). The responses are shown for the positive direction (pos.) that matches the experiment and for the negative direction (neg.) that corresponds to a continuation of the arms (see Fig. 1(a)).

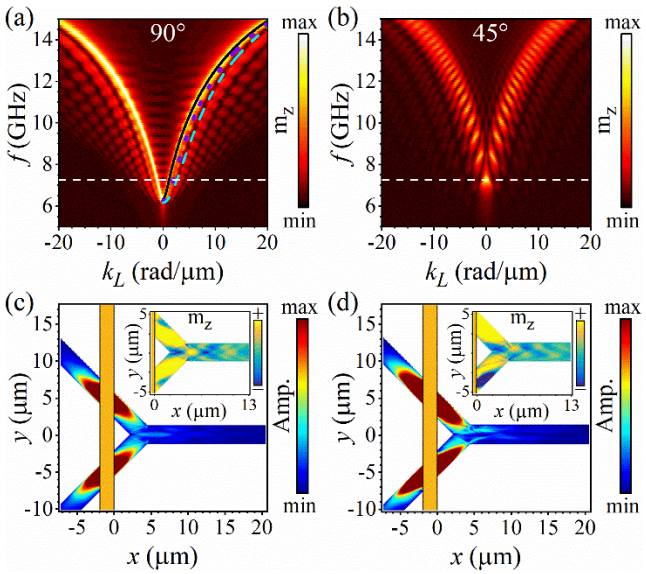

Figure 3: Spin wave dispersion curves obtained using micromagnetic simulations are shown for the (a) 90° and (b) 45° cases. Analytical calculations of the spin wave dispersion relations for the three lowest-order, odd, width-quantized modes are superimposed in (a) for $k_L > 0$ (black straight, purple dotted, and blue dashed are for modes n = 1, 3, and 5, respectively), and horizontal dashed lines at f = 7.25 GHz are shown in (a) and (b). Spin wave amplitude maps at f = 7.25 GHz for the Y case are shown in (c) and (d) with H applied along the antenna and at an angle of $-3°$ with respect to the antenna, respectively. The insets show corresponding snapshots of m_z at an instant in time.